Formulating Wave Overtopping at Vertical and Sloping Structures with Shallow Foreshores Using Deep-Water Wave Characteristics

Christopher H. Lashley[1]; Jentsje van der Meer, M.ASCE[2]; Jeremy D. Bricker[3]; Corrado Altomare[4]; Tomohiro Suzuki[5]; and Katsuya Hirayama[6]

Abstract: The state-of-the-art formulas for mean wave overtopping (q) assessment typically require wave conditions at the toe of the structure as input. However, for structures built either on land or in very shallow water, obtaining accurate estimates of wave height and period at the structure toe often proves difficult and requires the use of either physical modeling or high-resolution numerical wave models. Here, we follow Goda's method to establish an accurate prediction methodology for both vertical and sloping structures based entirely on deep-water characteristics—where the influence of the foreshore is captured by directly incorporating the foreshore slope and the relative water depth at the structure toe ($h_{toe}/H_{m0,deep}$). Findings show that q decreases exponentially with $h_{toe}/H_{m0,deep}$ due to the decrease of the incident wave energy; however, the rate of reduction in q decreases for structures built on land or in extremely shallow water ($h_{toe}/H_{m0,deep} \leq 0.1$) due to the increased influence of wave-induced setup and infragravity waves—which act as long-period fluctuations in mean water level—generated by nonlinear wave transformation over the foreshore. **DOI: [10.1061/(ASCE)WW.1943-5460.0000675](#)**. *This work is made available under the terms of the Creative Commons Attribution 4.0 International license, https://creativecommons.org/licenses/by/4.0/.*

Author keywords: Infragravity waves; Vertical wall; Emergent toe; Dike; Shallow foreshore; Wave transformation; Wave overtopping.

Introduction

Background

Coastal engineers rely on empirical formulas to predict the volume of water that passes over the crest of coastal structures due to wave action during storms. This process, known as wave overtopping, can result in damage to critical infrastructure and even loss of life. Despite recent studies which suggest that the flow properties of individual overtopping events are equally important (Altomare et al. 2020a; Sandoval and Bruce 2018; Suzuki et al. 2020), coastal structures worldwide are typically designed to resist a mean overtopping discharge per meter width of structure, q (m³/s or l/s per m)—which is often estimated using empirical formulas.

The state-of-the-art empirical models for wave overtopping of sloping structures (EurOtop 2018), including that of Altomare et al. (2016) and Van Gent (1999) developed specifically for shallow foreshores, typically require wave parameters at the toe of the structure as input—namely significant wave height ($H_{m0,toe}$) and spectral wave period ($T_{m-1,0,toe}$). The general assumption is that if the wave heights and periods at the toe are known, then the influence of directional spreading (Altomare et al. 2020b), local wind, and the foreshore—irregular or uniform—on wave characteristics is already accounted for. However, one major drawback is that for very shallow conditions, with heavy wave breaking, obtaining accurate estimates at the toe typically requires either physical model tests or high-resolution numerical models capable of capturing the nonlinear effects of wave transformation over the foreshore (Mase et al. 2013).

In addition to a rise in mean water level known as wave-induced (static) setup ($\bar{\eta}$), the shoaling and subsequent breaking of incident wind-sea and swell (SS) waves result in the generation and release of much longer waves, referred to as infragravity (IG) waves (or dynamic setup). These waves with periods exceeding 25 s not only contribute to $H_{m0,toe}$ but also result in higher values of $T_{m-1,0,toe}$ (Hofland et al. 2017). Lashley et al. (2020a) showed that the relative magnitude of IG waves at the structure is largely dependent on the foreshore slope (tan (m)) and the ratio of initial water depth at the toe to the offshore wave height ($h_{toe}/H_{m0,deep}$), with a large amount of IG-wave energy expected under *very shallow*

[1]Ph.D. Researcher, Dept. of Hydraulic Engineering, Delft Univ. of Technology, Stevinweg 1, 2628 CN Delft, Netherlands (corresponding author). ORCID: https://orcid.org/0000-0001-7149-2864. Email: c.h.lashley@tudelft.nl

[2]Principal, Van der Meer Consulting, P.O. Box 11, 8490 AA Akkrum, Netherlands; Professor, Coastal & Urban Risk & Resilience Dept., IHE Delft, Westvest 7, 2611 AX Delft, Netherlands. Email: jm@vandermeerconsulting.nl

[3]Associate Professor, Dept. of Hydraulic Engineering, Delft Univ. of Technology, Stevinweg 1, 2628 CN Delft, Netherlands; Associate Professor, Dept. of Civil and Environmental Engineering, Univ. of Michigan, 2350 Hayward St., Ann Arbor, MI 48109-2125. Email: jeremydb@umich.edu

Note. This manuscript was submitted on February 17, 2021; approved on July 13, 2021; published online on August 31, 2021. Discussion period open until January 31, 2022; separate discussions must be submitted for individual papers. This paper is part of the ***Journal of Waterway, Port, Coastal, and Ocean Engineering***, © ASCE, ISSN 0733-950X.

[4]Marie Curie Postdoctoral Fellow, Maritime Engineering Laboratory, Dept. of Civil and Environmental Engineering, Universitat Politècnica de Catalunya—BarcelonaTech, C/Jordi Girona 1-3, Edifici D1, Campus Nord, 08034 Barcelona, Spain. ORCID: https://orcid.org/0000-0001-8817-0431. Email: corrado.altomare@upc.edu

[5]Researcher, Flanders Hydraulics Research, Berchemlei 115, 2140 Antwerp, Belgium; Visiting Researcher, Dept. of Hydraulic Engineering, Delft Univ. of Technology, Stevinweg 1, 2628 CN Delft, Netherlands. ORCID: https://orcid.org/0000-0002-6008-4440. Email: tomohiro.suzuki@mow.vlaanderen.be

[6]Head of Wave Group, Coastal and Ocean Engineering Dept., Port and Airport Research Institute, 3-1-1, Nagase, Yokosuka, Kanagawa 239-0826, Japan. Email: hirayama@p.mpat.go.jp

conditions $(0.3 < h_{\text{toe}}/H_{m0,\text{deep}} < 1)$ and IG-wave dominance expected under *extremely shallow* conditions $(h_{\text{toe}}/H_{m0,\text{deep}} < 0.3)$—as defined by Hofland et al. (2017). Therefore, any numerical model applied to such shallow-water conditions must be capable of resolving both SS- and IG-wave motions. This means that the typical approach of using spectral wave models (e.g., SWAN) is no longer valid and that more computationally demanding, phase-resolving models are required (e.g., SWASH, XBeach, or BOSZ) (Lashley et al. 2020b).

Noting these challenges, Mase et al. (2013) developed a set of unified run-up and overtopping formulas, recently improved by Yuhi et al. (2020), for sloping structures under very shallow conditions with the deep-water wave height $(H_{m0,\text{deep}})$ and deep-water peak period (T_p) as main input. However, the approach has two notable drawbacks: first, the formulas directly relate wave overtopping to wave run-up. While this is physically justified, it requires the user to first accurately estimate wave run-up before estimating q. Second, the formulas are highly sensitive to the estimated water depth at the onset of wave breaking—which may vary depending on the wave transformation model or method used to estimate it. In light of this, Tamada et al. (2015) proposed a set of formulas to estimate the water depth at the onset of breaking, which were empirically derived with numerical model tests using a hybrid frequency-domain KdV equation developed by Mase and Kirby (1993).

For vertical structures fronted by very shallow foreshores, the design diagrams of Goda et al. (1975)—which use *equivalent* deep-water wave parameters—are considered as the technical standard for the design of port and harbor facilities in Japan. Ultimately, the drawn curves were the combined result of: a basic equation of wave overtopping (Goda 1970); a wave deformation model for random waves; and an engineering judgment, considering the effects of wave setup and IG waves (Goda et al. 1975). As a result, no empirical formula was developed to match the drawn curves. The significant advantage of this approach is that no additional wave transformation model (numerical or empirical) is required and the foreshore's influence is directly taken into account by its relative water depth and slope—which is assumed to be uniform. This uniform slope in the method is a drawback compared to the EurOtop (2018) method. While this approach is widely recognized and respected, graphical methods are typically more time-consuming, susceptible to human error, and difficult to automate for large-scale application than formulas. In light of this, a set of semitheoretical formulas which approximate the Goda et al. (1975) design diagrams, proposed by Takayama et al. (1982), is sometimes applied in Japan.

In the present study, we aim to resolve these challenges by establishing empirical overtopping formulas for both vertical and sloping structures with very shallow foreshores; formulas which are based entirely on deep-water characteristics and therefore do not require the use of any additional empirical or numerical models. This is achieved by revisiting the approach of Goda et al. (1975) which suggests that q can be accurately modeled as a function of relative water depth $(h_{\text{toe}}/H_{m0,\text{deep}})$, foreshore slope (m), and deep-water wave steepness (s_{op}).

Outline

This paper is organized as follows: the "Methods" section provides an overview of the existing empirical methods for wave transformation and overtopping under very shallow conditions, followed by descriptions of the numerical and physical model data sets considered. The "Methods" section also describes the performance metrics used to carry out the analyses. In the "Results and Discussion" section, the influence of the foreshore on nearshore wave conditions—and by extension the importance of $h_{\text{toe}}/H_{m0,\text{deep}}$ and tan (m)—is presented and discussed. Following this, new empirical formulas for both vertical and sloping structures fronted by shallow foreshores are derived and compared to existing approaches. The "Conclusions" section concludes the paper by addressing the overall research objective, stating limitations, and identifying areas for future work.

Methods

Existing Empirical Methods for Very Shallow Water

Goda's Empirical Wave Model

Goda et al. (1975) applied the following empirical expression to estimate the root-mean-square amplitude of IG waves (surfbeat)—also referred to as dynamic wave setup—within the surf zone (ζ_{rms}). This expression corresponds to Eq. (3.24) in Goda (2000), published as the book's second edition. It should be noted that the first edition was published in Goda (1985) and the third edition subsequently in Goda (2010):

$$\zeta_{\text{rms}} = \frac{0.01 \cdot H_{m0,\text{deep}}}{\sqrt{s_{op}(1 + (h_{\text{toe}}/H_{m0,\text{deep}}))}} \tag{1}$$

In Japanese research, reference is often made to an equivalent deep-water wave (H_0') to describe deep-water waves which have been adjusted to account for the effects of refraction, diffraction, and other transformations—excluding wave shoaling and breaking (Goda 2000). In the present study, considering 1D numerical and physical model tests with long-crested waves, H_0' and $H_{m0,\text{deep}}$ are considered to be the same quantity.

Here, we assume that the IG-wave height is twice the IG-wave amplitude, and thus,

$$H_{m0,\text{IG}} = \sqrt{2} \cdot 2 \cdot \zeta_{\text{rms}} \tag{2}$$

Note that $\sqrt{2}$ is used to convert the root-mean-square wave height to the significant wave height. Despite it being a significant advancement, Goda (2000) acknowledged that Eq. (1) was an engineering estimate and expected that future random-wave-breaking models would directly include the effects of IG waves for more accurate and rational predictions in the surf and swash zones.

While other random-wave transformation models at the time completely neglected the influence of IG waves (Battjes and Stive 1985; Dally 1992), Goda (2000) was able to account for the effects of IG waves on SS-wave transformation in the surf zone—assessed as the change in $H_{1/3}$—by expressing the IG waves as an increase in the local water depth by ζ_{rms} [Eq. (1)] which, in turn, controls the breaker height:

$$H_{1/3} = \begin{cases} K_s \cdot H_{m0,\text{deep}} & : \frac{h_{\text{toe}}}{L_0} \geq 0.2 \\[2ex] \min\{(\beta_0 \cdot H_{m0,\text{deep}} + \beta_{\max} \cdot h_{\text{toe}}), \ \beta_{\max} \cdot H_{m0,\text{deep}}, \ K_s \cdot H_{m0,\text{deep}}\} & : \frac{h_{\text{toe}}}{L_0} < 0.2 \end{cases} \tag{3}$$

where $H_{1/3}$ is considered the mean of the highest one-third of SS waves; K_s is the shoaling coefficient, and

$$\beta_0 = 0.028 \cdot s_{op}^{-0.38} \exp\left(20 \cdot \tan(m)^{1.5}\right) \quad (4)$$

$$\beta_1 = 0.52 \cdot \exp\left(4.2 \cdot \tan(m)\right) \quad (5)$$

and

$$\beta_{\max} = \max\{0.92, 0.32 \cdot s_{op}^{-0.29} \cdot \exp\left(2.4 \tan(m)\right)\} \quad (6)$$

Note that Eq. (3) corresponds to Eq. (3.25) in Goda (2000). It is also worth noting that while Goda (2000) looked at $H_{1/3}$—obtained using a zero-crossing analysis of the surface elevation time series—we focus on H_{m0}—obtained using spectral analysis—in the present study. In deep water, $H_{1/3} \approx H_{m0}$ when wave refraction and diffraction are negligible; however, the two quantities can differ significantly for breaking waves in the surf zone. Our choice to focus on H_{m0} here is consistent with the current European standard (EurOtop 2018) and is based on the fact that most operational forecast models provide H_{m0} as output.

Wave Overtopping

In general, there are two approaches to estimating wave overtopping. The first one, which is adopted by EurOtop (2018) for sloping structures, uses wave parameters at the toe of the structure as input. The second approach—proposed by Goda et al. (1975)—uses deep-water parameters to estimate q. In this approach, the effects of the foreshore are represented by two foreshore parameters: $h_{toe}/H_{m0,deep}$ and m.

EurOtop (2018) Approach. EurOtop (2018), with the work of Van Gent (1999) and Altomare et al. (2016) for sloping structures in shallow water, make use of the following formulas:

$$\frac{q}{\sqrt{g \cdot H_{m0,toe}^3}} = 0.16 \cdot \exp\left(-\frac{R_c}{H_{m0,toe}} \cdot \frac{1}{(0.33 + 0.022 \cdot \xi_{m-1,0})}\right) \quad (7)$$

where R_c = crest freeboard and $\xi_{m-1,0}$ = breaker parameter. For shallow foreshores with $h_{toe}/H_{m0,deep} < 1$,

$$\xi_{m,-1,0} = \frac{\tan(\delta)}{\sqrt{s_{om-1,0}}} \quad (8)$$

where $s_{om-1,0} = H_{m0,toe}/L_{m-1,0}$ and

$$L_{m-1,0} = \frac{g \cdot T_{m-1,0,toe}^2}{2\pi} \quad (9)$$

For cases where $T_{m-1,0,toe}$ is unknown, it may be estimated by its deep-water equivalent using the empirical formulas of Hofland et al. (2017). The *equivalent slope* (δ), used to calculate the breaker parameter, $\xi_{m-1,0}$, is given by

$$\tan(\delta) = \frac{1.5 \cdot H_{m0,toe} + R_{u2\%}}{(1.5 \cdot H_{m0,toe} - h_{toe}) \cdot \cot(m) + (h_{toe} + R_{u2\%}) \cdot \cot(\alpha)} \quad (10)$$

where α = structure slope, and

$$\frac{R_{u2\%}}{H_{m0,toe}} = 4 - \frac{1.5}{\sqrt{\xi_{m-1,0}}} \quad (11)$$

Note that $\xi_{m-1,0}$ and $R_{u2\%}$ must also be obtained iteratively (until $R_{u2\%}$ converges), with a first estimate of $R_{u2\%} = 1.5 \cdot H_{m0,toe}$. It should also be noted that the data used by Altomare et al. (2016) were mainly based on foreshores with slopes (m ranging

from 1:250 to 1:35). Therefore, the applicability of Eqs. (7)–(11) to steeper slopes is yet to be confirmed.

Goda et al. (1975) Approach. Goda et al. (1975) developed design diagrams [Figs. 28 and 29 in Goda et al. (1975)] for smooth vertical walls (without roughness elements) and walls covered with sloping rubble-mound (made of armor blocks) with steep foreshores (tan $(m) = 1:10$ and $1:30$), which were subsequently published as Figs. 5.1, 5.2, 5.4 and 5.5 in Goda (2000). These design diagrams were based on the following equation:

$$\frac{q}{\sqrt{2 \cdot g \cdot H_{m0,deep}^3}} = f\left(\frac{h_{toe}}{H_{m0,deep}}, \frac{R_c}{H_{m0,deep}}, s_{op}, m\right) \quad (12)$$

In the present study, we focus on smooth structures under very shallow conditions; therefore, we focus on the diagrams developed for vertical walls with $h_{toe}/H_{m0,deep} < 1$.

Note that digitized sections of the Goda et al. (1975) design diagrams are shown in Figs. 7 and 8 as part of the analysis (see the "Results and Discussion" section).

Description of Data Sets

A comprehensive collection of physical and numerical model data sets, with different foreshore slopes, structure slopes, offshore wave conditions, and relative water depths, were considered in this study. Data sets with measurements both offshore and at the structure toe were used to assess the influence of the foreshore on incident wave conditions, while data sets with overtopping measurements for normally incident waves over smooth sloping or vertical structures that met the criteria for very shallow conditions ($h_{toe}/H_{m0,deep} \leq 1$) were used in the development of a new overtopping formulas.

The reference, identifier (ID), number of tests, and range of parameters for each data set are provided in Tables 1–3. Each of the selected data sets followed Fig. 1, in terms of layout, with uniformly sloping foreshore slopes under irregular, long-crested, and shore-normal wave attack. Rather than providing a lengthy and exhaustive description here, we focus on two data sets: (1) the Goda et al. (1975) data set (DS-802)—which makes up the bulk of the available vertical wall data; and (2) the Lashley et al. (2020a) data set (XB)—which, unlike the others, is comprised of purely numerical model results. For detailed descriptions of the other data sets, the reader is pointed to the references listed in Tables 1–3 for the details related to each individual test setup. The data sets with an ID prefix DS refer to tests obtained from the CLASH project (Crest Level Assessment of Coastal structures by full-scale monitoring, neural network prediction, and hazard analysis on permissible wave overtopping) database, see also EurOtop (2018). Note that some of the tests within the CLASH database were listed as confidential, therefore no references for these tests were available. Additionally, it should be noted that 1:1,000 foreshore slope in the CLASH database refers to a completely flat foreshore in reality.

It is important to note that by using data sets collected from different facilities around the world, additional differences may arise due to model effects and different measurement techniques. Therefore, a certain degree of spread in the compiled data set is to be expected and accepted as inherent in the approach taken.

Goda et al. (1975) Data Set

Goda et al. (1975) carried out a series of experiments in 1973 and 1974 with irregular waves (Bretschneider–Mitsuyasu type spectrum), with $H_{1/3} = 0.15$ m and $T_{1/3} = 1.7$, 2.3, and 2.8 s,

Table 1. Summary of parameter ranges for the data sets used to assess the effect of the foreshore on incident waves

Reference	ID	No. of tests	$s_{m-1,0}$	$h_{toe}/H_{m0,deep}$	cot (m)
—	Sal	13	0.018–0.039	1.53–5.19	30
Smith et al. (2003)	Smith	114	0.017–0.052	0.36–5.96	30; 100
Lashley et al. (2020a)	XB	384	0.006–0.041	0.05–5	10; 25; 50; 100; 250; 500; 1,000
Coates et al. (1997)	HR	161	0.008–0.058	0.46–4.63	10; 20; 30; 50
—	DS-005	15	0.016–0.028	1.4–1.67	100
—	DS-111	81	0.002–0.036	1.27–5.08	50
Van der Meer and de Waal (1993)	DS-221	148	0.011–0.059	0.97–6.87	100; flat
—	DS-307	18	0.042–0.043	0.98–2.28	250
—	DS-330	12	0.046–0.062	1.87–3.38	100
Pullen and Allsop (2004)	DS-509	18	0.048–0.09	1.08–1.60	50
—	DS-916	47	0.015–0.048	1.34–2.65	30

Table 2. Summary of parameter ranges for the data sets used to assess the effect of the foreshore on incident waves and wave overtopping for sloping structures; the number of tests with $h_{toe}/H_{m0,deep} \leq 0.1$ is parenthesized

Reference	ID	No. of tests	$s_{om-1,0}$	$h_{toe}/H_{m0,deep}$	cot (m)	cot (α)	$R_c/H_{m0,deep}$
Altomare et al. (2016)	13–116	90 (60)	0.015–0.063	−0.06–0.22	35	3	0.40–0.82
	00–025	21 (17)	0.039–0.041	−0.14–0.25	35	2	0.24–0.67
	00–142	17	0.013–0.036	0.25–0.5	35	3	0.22–0.52
	13–168	42 (15)	0.007–0.018	0–0.86	50	2	0.26–2.55
Goda (2009) and Tamada et al. (2002)	Tam	198 (37)	0.019–0.049	0–0.71	10; 30	3; 5; 7	0.31–1.50
Van Gent (1999)	DS-226	97	0.018–0.053	0.32–2.56	100; 250	2.5; 4	1.1–2.9

Table 3. Summary of parameter ranges for the data sets used to assess wave overtopping for vertical structures; the number of tests with $h_{toe}/H_{m0,deep} \leq 0.1$ is parenthesized

Reference	ID	No. of tests	$s_{om-1,0}$	$h_{toe}/H_{m0,deep}$	cot (m)	$R_c/H_{m0,deep}$
Goda et al. (1975)	DS-802	127 (44)	0.005–0.044	−0.75–1	10; 30	0.40–1.92
Herbert (1993)	DS-028	24	0.018–0.049	0.49–0.97	10; 100	0.48–2.07
Bruce et al. (2002)	VOWS	10	0.027–0.072	0.81–0.99	10; 50	0.76–1.65
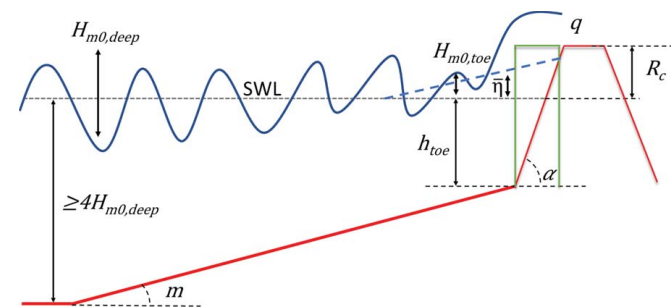
Fig. 1. Schematic representation of vertical and sloping structures with very shallow foreshores, highlighting key variables.

overtopping a vertical structure fronted by 1:10 and 1:30 sloping foreshores. Incident wave heights were estimated with a technique to resolve incident and reflected waves using two simultaneous wave records. The overtopping rate was obtained as the average of three measurements, each for 200 waves.

The original data set comprised consisted of 205 tests with conditions at the toe varying from shallow to emergent, where the toe of the structure was initially dry ($h_{toe} \leq 0$). Here, we analyze a subset of these tests with $h_{toe}/H_{m0,deep} \leq 1$ (DS-802, Table 3).

Goda et al. (1975) noted that during the physical tests, the amplitude of the IG waves [estimated at the time using Eq. (1)] and the level of wave-induced setup were higher than those typically observed at a

real coast. This was attributed to the re-reflection of waves between the vertical wall and the wave generation paddle, the magnitude of which varied depending on tan (m) and $h_{toe}/H_{m0,deep}$. This modification was based on engineering judgment, not measurements.

To compensate for this, Goda et al. (1975) increased the measured h_{toe}—and by relation reduced R_c—by the values shown in Table 4 based on engineering judgment, not measurements. These corrected values were then used to derive the design diagrams presented in Goda (2000) which have since been adopted in the technical standard for the design of port and harbor facilities in Japan. To be consistent with this analysis, we have applied the same correction to the original data here.

Lashley et al. (2020a) Data Set
After verifying the numerical model's ability to accurately simulate wave transformation under very shallow conditions, Lashley et al. (2020a) carried out 672 simulations in prototype scale—using the XBeach nonhydrostatic numerical model (Kingsday release)—of irregular waves [Joint North Sea Wave Project (JONSWAP) type with a peak enhancement factor of 3.3] propagating over an idealized structure-foreshore profile (Fig. 1). In these simulations, $H_{m0,deep}$, T_p, wave directional spreading, h_{toe}, m, bottom friction, width of vegetated cover, and structure slope (α) were systematically varied, following a one-[factor]-at-a-time (OAT) approach. In the present study, we analyze a part of this data set, without the influence of vegetation, directional spreading, bottom friction, or wave reflection (i.e., with the structure removed). In each simulation, $H_{m0,toe}$, $T_{m-1,0,toe}$, wave-induced setup at the structure toe ($\bar{\eta}$), and the relative

Table 4. Correction to h_{toe} and R_c in cm as proposed by Goda et al. (1975)

h_{toe} (cm)	tan $(m) = 1:30$			tan $(m) = 1:10$		
	$T_{1/3} = 1.7$ s	$T_{1/3} = 2.3$ s	$T_{1/3} = 2.8$ s	$T_{1/3} = 1.7$ s	$T_{1/3} = 2.3$ s	$T_{1/3} = 2.8$ s
22.5	1.5	1.5	1.5	1.5	1.5	1.5
15.0	1.5	1.5	1.5	1.5	1.5	1.5
10	1.5	1.5	1.5	1.5	1.5	1.5
5	1.5	1.5	1.5	1.5	2	2
0	1.5	1.5	1.5	2	2.5	2.5
−5	1.5	1.5	1.5	2	2.5	2.5
−10	—	—	—	2	2.5	2.5

magnitude of the IG waves, defined as the ratio of IG to SS waves at the structure toe ($H_{m0,IG,toe}/H_{m0,SS,toe}$), were assessed.

In each simulation, the offshore water depth was set to four times $H_{m0,deep}$, in line with the definition of deep water proposed by Hofland et al. (2017). The numerical model was configured such that the numerical parameter governing the maximum breaking wave steepness was set to 0.5; a smooth flume bottom was represented using a Manning roughness coefficient of 0.012 s/m$^{1/3}$; and a cross-shore grid spacing varying from a maximum of 100-grid cells per deep-water wavelength (offshore) to 1 m at the toe.

Performance Metrics

In order to assess the performance of the empirical model for relative wave height at the toe ($H_{m0,toe}/H_{m0,deep}$), the Scatter Index (SCI) objective function was applied as a normalized measure of error:

$$\text{SCI}_\Psi = \frac{\sqrt{(1/N) \sum_{i=1}^{N} (\Psi_{pred}^i - \Psi_{meas}^i)^2}}{(1/N) \sum_{i=1}^{N} \Psi_{meas}^i} \quad (13)$$

where $\Psi = H_{m0,toe}/H_{m0,deep}$, in a sample size N; and subscripts pred and meas = to the empirical predictions and measurements, respectively. Lower SCI values (<0.2) indicate accurate model predictions.

Following Altomare et al. (2016), the geometric mean ($\bar{x}_G$) is applied to assess the accuracy of the overtopping formulas:

$$\bar{x}_G = \exp\left[\frac{1}{N} \sum_{i=1}^{N} \ln x_i\right] \quad (14)$$

with $x_i = q_{pred,i}/q_{meas,i}$, where N = number of data points, $q_{pred,i}$ and $q_{meas,i}$ = ith modeled (empirically) and observed mean overtopping discharges, respectively. A $\bar{x}_G$ value of 1 indicates no bias, while values greater than and less than 1 indicate tendencies to over- and underestimate q, respectively. Similarly, the geometric standard deviation associated with the mean is applied to assess the level of scatter—and general accuracy—of the empirical formulas:

$$\sigma(\bar{x}_G) = \exp\left\{\left[\frac{1}{N} \sum_{i=1}^{N} [(\ln x_i)^2 - (\ln \bar{x}_G)^2]\right]^{0.5}\right\} \quad (15)$$

If the data is assumed to be normally distributed, 90% of the data will fall within 1.65 standard deviations, with lower bound, $\bar{x}_G \cdot [\sigma(\bar{x}_G)^{-1.65}]$ and the upper bound, $\bar{x}_G \cdot [\sigma(\bar{x}_G)^{1.65}]$.

Results and Discussion

Foreshore Effect on Nearshore Conditions

In order to establish accurate wave overtopping formulas based on deep-water wave characteristics, the effects of shallow foreshores
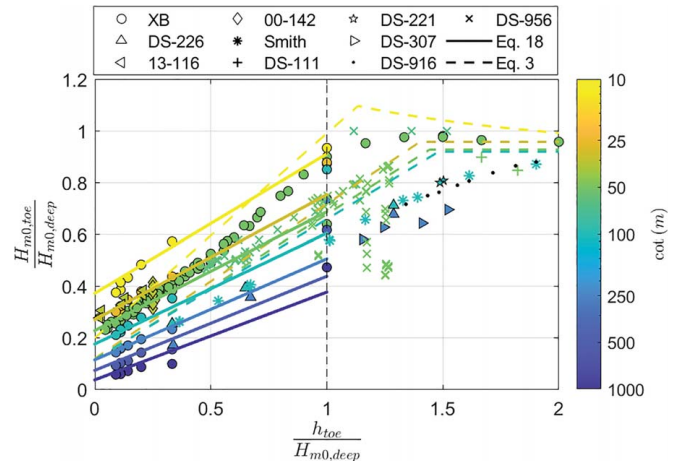

Fig. 2. Variation in relative wave height at the toe ($H_{m0,toe}/H_{m0,deep}$) with relative water depth at the toe ($h_{toe}/H_{m0,deep}$) and foreshore slope (cot (m)) (see shading scale) for data with $0.030 <$ wave steepness ($s_{om-1,0}$) < 0.042. The solid and dashed lines represent Eqs. (16) and (3), respectively, for $s_{om-1,0} = 0.036$.

on wave conditions at the toe of the structure need to be accurately parameterized. In this section, we demonstrate that the foreshore effects on nearshore conditions can be accurately modeled as functions of $h_{toe}/H_{m0,deep}$, tan (m) and $s_{om-1,0}$. The nearshore processes considered are, namely: (1) the change in significant wave height due to shoaling and breaking; and (2) the increase in static and dynamic wave setup (i.e., the magnitude of IG waves).

Significant Wave Height

Under very shallow conditions ($h_{toe}/H_{m0,deep} \leq 1$), two trends in Fig. 2 become evident: (1) $H_{m0,toe}/H_{m0,deep}$ decreases linearly as $h_{toe}/H_{m0,deep}$ decreases; and (2) $H_{m0,toe}/H_{m0,deep}$ increases as cot (m) becomes steeper (visible by the marker shading in Fig. 2). The area where $1 < h_{toe}/H_{m0,deep} \leq 1.5$ appears to be a transition region where the foreshore—represented by $h_{toe}/H_{m0,deep}$ and tan (m)—shows a minor influence on $H_{m0,toe}/H_{m0,deep}$.

In addition, Fig. 3 indicates that the influence of the deep-water wave steepness ($s_{om-1,0}$) on $H_{m0,toe}/H_{m0,deep}$ decreases as $h_{toe}/H_{m0,deep}$ decreases, made evident by the reduced scatter at lower $h_{toe}/H_{m0,deep}$ values. Note that $s_{om-1,0}$ is used here in place of s_{op} in accordance with the current standard, where $T_{m-1,0}$ is used in place of T_p or $T_{1/3}$ (EurOtop 2018); for conversion, we take $T_{m-1,0} = T_p/1.1$.

For conditions where $h_{toe}/H_{m0,deep} \leq 1$, the following expression holds with $R^2 = 0.84$ and SCI = 0.18 (Fig. 4):

$$\frac{H_{m0,toe}}{H_{m0,deep}} = M \cdot \frac{h_{toe}}{H_{m0,deep}} + C \quad (16)$$

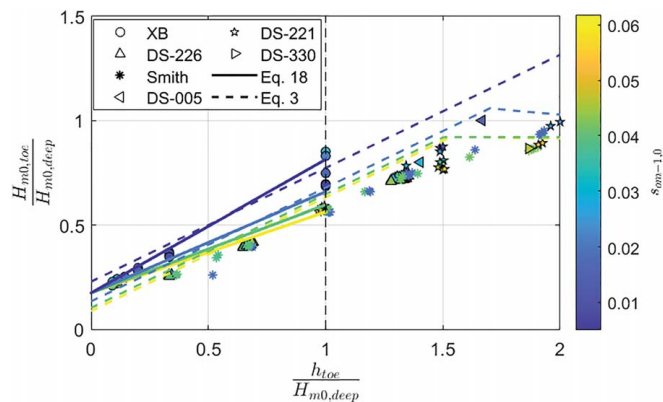**Fig. 3.** Variation in relative wave height at the toe ($H_{m0,\text{toe}}/H_{m0,\text{deep}}$) with relative water depth ($h_{\text{toe}}/H_{m0,\text{deep}}$) and wave steepness [($s_{om-1,0}$) shading scale] for data with foreshore slope (cot (m)) = 100. The solid and dashed lines represent Eqs. (16) and (3), respectively.
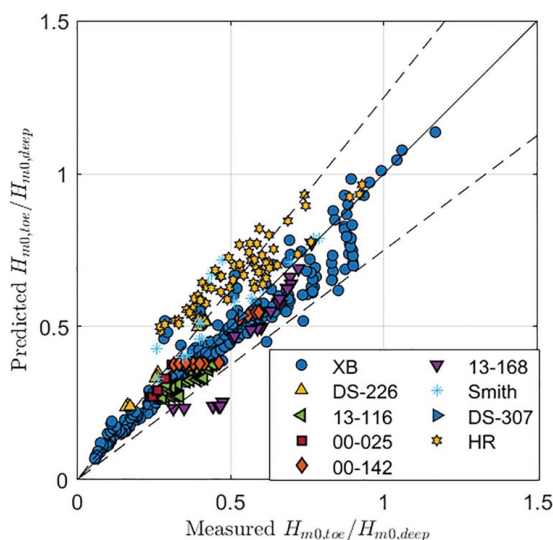

Fig. 4. Predicted [using Eq. (16)] versus measured $H_{m0,\text{toe}}/H_{m0,\text{deep}}$ for data with $h_{\text{toe}}/H_{m0,\text{deep}} \leq 1$ (Tables 1 and 2). The solid line indicates perfect agreement. The Dashed lines indicate ±25% error.

where

$$M = 0.35 \cdot \frac{\tan{(m)}^{0.10}}{s_{om-1,0}^{0.20}} \qquad (17)$$

and,

$$C = 0.95 \cdot \tan{(m)}^{0.15} - 0.30 \qquad (18)$$

Eqs. (16)–(18) were derived based on the observed linear relationship between $H_{m0,\text{toe}}/H_{m0,\text{deep}}$ and $h_{\text{toe}}/H_{m0,\text{deep}}$ where the slope (M) and intercept (C) of the relationship are dependent on $\tan{(m)}$ and $s_{om-1,0}$. The exponents of each term were then obtained using a trial-and-error approach to minimize scatter in the data (Table 1). It should be highlighted that $H_{m0,\text{toe}}/H_{m0,\text{deep}} \neq 0$ when $h_{\text{toe}}/H_{m0,\text{deep}} = 0$ due to the influence of static and dynamic setup (IG waves), discussed in the following section and also highlighted by Goda (2000). However, experience suggests that care should be taken for cases with $h_{\text{toe}}/H_{m0,\text{deep}} = 0$, as the bed may intermittently become dry.

As noted in the "Description of Data Sets" section of the "Methods", some scatter in Fig. 4 is to be expected due to model effects and differences in measurement techniques between data sets. In particular, the low-frequency cut-off used to calculate H_{m0} could significantly influence results under very shallow conditions where IG waves dominate.

Through Eq. (16), the wave height at the structure may be estimated using parameters that are usually either known or estimated without difficulty: the offshore wave height, offshore steepness, foreshore slope, and relative water depth at the structure toe. This is also directly in line with the work of Hofland et al. (2017) who showed that the relative wave period at the toe ($T_{m-1,0,\text{toe}}/T_{m-1,0,\text{deep}}$) can be empirically modeled, with reasonable accuracy, as a function of $h_{\text{toe}}/H_{m0,\text{deep}}$ and $\tan{(m)}$. The main disadvantage of such an empirical approach is the assumption of a straight (uniform) foreshore slope. However, this disadvantage is seen as minor compared with the use of numerical models that do not include IG waves in very shallow water, e.g., SWAN.

Given the differences in the approach of Goda (2000)—namely the use of $H_{1/3}$ and not H_{m0}, and the treatment of the IG waves as an increase in mean water level versus directly including them in the wave height estimate, as done here—our comparison of Eqs. (3) and (16) is purely qualitative. Both equations capture the linear relationship between $h_{\text{toe}}/H_{m0,\text{deep}}$ and $H_{m0,\text{toe}}/H_{m0,\text{deep}}$ and the increase in $H_{m0,\text{toe}}/H_{m0,\text{deep}}$ with steeper slopes. The main difference between the two approaches is the treatment of the deep-water wave steepness ($s_{om-1,0}$). Eq. (3) shows parallel lines for different values of $s_{om-1,0}$, while Eq. (16) converges as $h_{\text{toe}}/H_{m0,\text{deep}}$ decreases (Fig. 3). This convergence was observed in the data (Fig. 3) and is due to the depth-limited nature of shallow water waves. That is, as the water depth becomes shallower, the influence of $s_{om-1,0}$ decreases and the magnitude of $H_{m0,\text{toe}}$ is now governed by h_{toe}.

The observed convergence is also supported by the linear wave theory, which states that waves become less (frequency) dispersive as the water depth becomes shallower—that is, the influence of the wave period (and by extension $s_{om-1,0}$) on nearshore wave conditions decreases as $h_{\text{toe}}/H_{m0,\text{deep}}$ decreases. This is also made evident in Fig. 5 by the decrease in scatter with shallower water depths. Of particular note is the correspondence between $h_{\text{toe}}/H_{m0,\text{deep}} \leq 1$ and the definition of shallow water according to linear wave theory, where the ratio of the local water depth to wavelength ($h_{\text{toe}}/L_{\text{toe}}$) < 1/20 (Fig. 5), and L_{toe} is obtained by solving the well-known dispersion relationship.

Static and Dynamic Wave Setup
In addition to the relative wave height and period at the toe, $h_{\text{toe}}/H_{m0,\text{deep}}$ and $\tan{(m)}$ serve as descriptors for both the magnitude of relative (static) wave setup [$\bar{\eta}/H_{m0,\text{deep}}$, Fig. 6(a)] and the dynamic wave setup—represented by the relative magnitude of the IG waves at the toe [$H_{m0,\text{IG,toe}}/H_{m0,\text{SS,toe}}$, Fig. 6(b)]—generated due to SS waves shoaling and breaking over the foreshore. Furthermore, both quantities appear to reach their maximum because $h_{\text{toe}}/H_{m0,\text{deep}}$ approaches zero (Fig. 6). The trend in $\bar{\eta}/H_{m0,\text{deep}}$ is also supported by the work of Goda (2000) which was obtained by digitizing and interpolating between the curves of Fig. 3.25 of the same reference, although XBeach predictions are consistently lower than that of Goda (2000). These differences are likely due to the definition of $\bar{\eta}$: Goda (2000) refers to $\bar{\eta}$ at the shoreline, i.e., the mean water level in the swash zone (where $\bar{\eta}$ reaches its maximum), while XBeach estimates of $\bar{\eta}$ were taken in the surf zone (Lashley et al. 2020a).

As Eq. (1) does not consider the influence of the foreshore slope, it is more valuable to assess the best-fit trend of $H_{m0,\text{IG,toe}}$—predicted
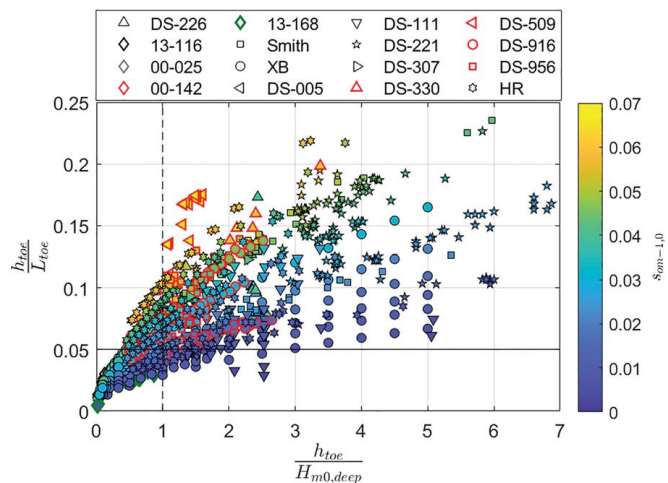
Fig. 5. Variation in ratio of local water depth to local wavelength—obtained by solving the well-known dispersion relationship—with relative water depth. Horizontal line indicates the transition to *shallow water* according to linear wave theory. The dashed vertical line indicates transition to very shallow conditions ($h_{toe}/H_{m0,\text{deep}} = 1$) according to Hofland et al. (2017).
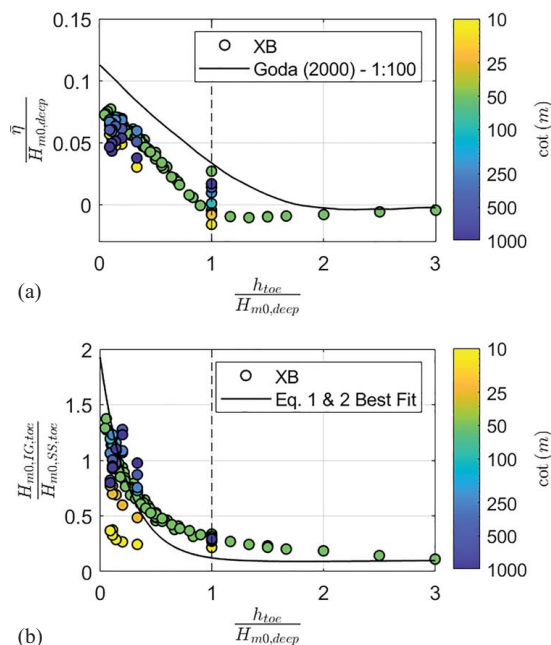

Fig. 6. Variation in (a) relative wave setup ($\bar{\eta}/H_{m0,\text{deep}}$); and (b) relative magnitude of infragravity waves ($H_{m0,IG,\text{toe}}/H_{m0,SS,\text{toe}}$) with relative water depth ($h_{toe}/H_{m0,\text{deep}}$) and foreshore slope (cot (m)), for data with $0.030 <$ wave steepness ($s_{om-1,0}$) < 0.042, as modeled numerically using XBeach nonhydrostatic. The solid line in panel *a* is based on $s_{om-1,0} = 0.036$.

using Eqs. (1) and (2)—normalized by $H_{m0,SS,\text{toe}}$ (predicted by XBeach). Remarkably, the best-fit trend of Eqs. (1) and (2) agrees well with the XBeach model results [Fig. 6(b)].

One important takeaway is that the influence of the foreshore only becomes significant once $h_{toe}/H_{m0,\text{deep}} \leq 1$; that is, all of the nearshore processes considered here: change in wave height (Figs. 2 and 3), change in wave period (Hofland et al. 2017), wave setup [Fig. 6(a)] and shift in energy to low frequencies

[Fig. 6(b)] show high correlations with $h_{toe}/H_{m0,\text{deep}}$ and tan (m) when $h_{toe}/H_{m0,\text{deep}} \leq 1$. So, in short, if $h_{toe}/H_{m0,\text{deep}} > 1$, then the foreshore may be neglected in the analysis and the EurOtop (2018) approach is practical. However, if $h_{toe}/H_{m0,\text{deep}} \leq 1$, wave shoaling and breaking become significant and a more accurate approach would be that of Goda et al. (1975).

Development of Overtopping Formulas

In the "Foreshore Effect on Nearshore Conditions" section of the "Results and Discussion," we demonstrated and discussed how the effects of the foreshore on nearshore conditions can be accurately represented as functions of $h_{toe}/H_{m0,\text{deep}}$ and tan (m). This suggests that wave overtopping, which is typically estimated as a function of nearshore parameters (at the toe of the structure), may actually be represented as a function of deep-water parameters when $h_{toe}/H_{m0,\text{deep}} \leq 1$. In line with the approach of Goda et al. (1975), also published in Goda (2000), we propose the following for vertical structures:

$$\frac{q}{\sqrt{g \cdot H_{m0,\text{deep}}^3}} = f\left(\frac{h_{toe}}{H_{m0,\text{deep}}}, \frac{R_c}{H_{m0,\text{deep}}}, s_{om-1,0}, \tan(m)\right) \quad (19)$$

Likewise, for sloping structures:

$$\frac{q}{\sqrt{g \cdot H_{m0,\text{deep}}^3}} = f\left(\frac{h_{toe}}{H_{m0,\text{deep}}}, \frac{R_c}{H_{m0,\text{deep}}}, s_{om-1,0}, \tan(m), \tan(\alpha)\right)$$

$$(20)$$

Vertical Structures
The data sets listed in Table 3 show a negative exponential relationship between relative discharge and relative freeboard (Fig. 7). This typical relationship is evident by the linear increase in $q/\sqrt{g \cdot H_{m0,\text{deep}}^3}$ (logarithmic y-axis) with decreasing freeboard (see light to dark gradations in shading). On the contrary, $q/\sqrt{g \cdot H_{m0,\text{deep}}^3}$ shows a positive and much more dynamic relationship with $h_{toe}/H_{m0,\text{deep}}$. Visual inspection of the data and original Goda et al. (1975) design diagrams revealed three distinct regimes: (1) a very shallow regime ($0.5 \leq h_{toe}/H_{m0,\text{deep}} \leq 1$), where a steep linear relationship exists between $\log\left(q/\sqrt{g \cdot H_{m0,\text{deep}}^3}\right)$ and $h_{toe}/H_{m0,\text{deep}}$; (2) an extremely shallow or emergent regime ($h_{toe}/H_{m0,\text{deep}} \leq 0.1$), where the relationship is much gentler—suggesting a reduced dependence; and (3) a transition region between the two regimes $(0.1 < h_{toe}/H_{m0,\text{deep}} < 0.5)$, where the rate of reduction $q/\sqrt{g \cdot H_{m0,\text{deep}}^3}$ with change in $h_{toe}/H_{m0,\text{deep}}$ is maximum. Notably, this transition region is centered on the threshold between very and extremely shallow water, $h_{toe}/H_{m0,\text{deep}} = 0.3$ (Hofland et al. 2017).

As noted in the "Foreshore Effect on Nearshore Conditions" section and Fig. 6, both static wave setup and dynamic setup—that is, the slow periodic variations in mean water level due to IG waves—increase considerably as $h_{toe}/H_{m0,\text{deep}}$ decreases. These static and periodic changes in mean water level equate to a reduction in $R_c/H_{m0,\text{deep}}$ which results in higher-than-expected overtopping for cases with $h_{toe}/H_{m0,\text{deep}} \leq 0.1$, as also observed by Goda et al. (1975).

Based on the aforementioned trends, the proposed formulas for vertical structures each have the following basic form:

$$\frac{q}{\sqrt{g \cdot H_{m0,\text{deep}}^3}} = a \cdot \exp\left(-b \cdot \frac{R_c}{H_{m0,\text{deep}}} + c \cdot \frac{h_{toe}}{H_{m0,\text{deep}}}\right) \quad (21)$$
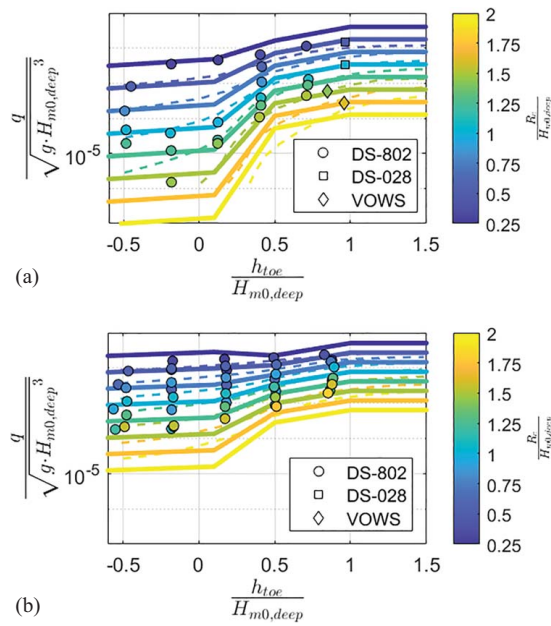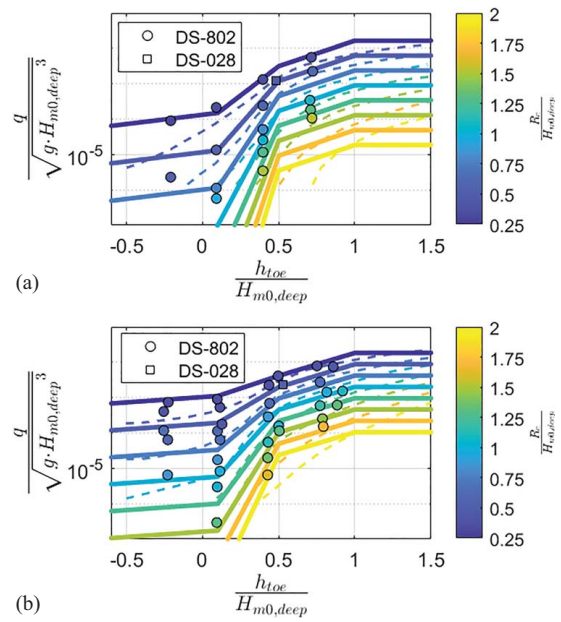
Fig. 7. Variation in relative discharge, $q/\sqrt{g \cdot H_{m0,deep}^3}$, with relative water depth ($h_{toe}/H_{m0,deep}$) and relative freeboard ($R_c/H_{m0,deep}$) for vertical structures (Table 3) with wave steepness ($s_{om-1,0}$): (a) 0.044; and (b) 0.015 for a foreshore slope (cot (m)) = 10. The solid lines represent Eqs. (21)–(28), whereas the dashed lines represent the digitized design curves of Goda et al. (1975).

Fig. 8. Variation in relative discharge, $q/\sqrt{g \cdot H_{m0,deep}^3}$, with relative water depth ($h_{toe}/H_{m0,deep}$) and relative freeboard ($R_c/H_{m0,deep}$) for vertical structures (Table 3) with wave steepness ($s_{om-1,0}$): (a) 0.044; and (b) 0.015, for a foreshore slope (cot (m)) = 30. The solid lines represent Eqs. (21)–(28), whereas the dashed lines represent the digitized design curves of Goda et al. (1975).

where the coefficients a, b, and c are each a function of $s_{om-1,0}$ and m. For very shallow cases (Regime 1), with $0.5 \leq h_{toe}/H_{m0,deep} \leq 1$:

$$a_1 = 0.90 \cdot \frac{\tan(m)^{2.05}}{s_{om-1,0}^{0.20}} \tag{22}$$

$$b_1 = 5.10 \cdot \frac{s_{om-1,0}^{0.25}}{\tan(m)^{0.15}} \tag{23}$$

and

$$c_1 = 0.70 \cdot \frac{s_{om-1,0}^{0.10}}{\tan(m)^{0.55}} \tag{24}$$

For extremely shallow or emergent cases (Regime 2), with $h_{toe}/H_{m0,deep} \leq 0.1$:

$$a_2 = 0.09 \cdot \frac{\tan(m)^{2.35}}{s_{om-1,0}^{1.25}} \tag{25}$$

$$b_2 = 5.40 \cdot \frac{s_{om-1,0}^{0.30}}{\tan(m)^{0.45}} \tag{26}$$

and

$$c_2 = 0.75 \cdot \frac{s_{om-1,0}^{0.50}}{\tan(m)^{0.60}} \tag{27}$$

For the transition between the two regimes ($0.1 < h_{toe}/H_{m0,deep} < 0.5$), the user should interpolate exponentially:

$$y_3 = y_2 \cdot \left(\frac{y_1}{y_2}\right)^{(x_3-x_2)/(x_1-x_2)} \tag{28}$$

where x and y are stand-ins for $h_{toe}/H_{m0,deep}$ and $q/\sqrt{g \cdot H_{m0,deep}^3}$, respectively; and the subscripts 1, 2, and 3 refer to the first, second, and transition (third) regimes, respectively.

Qualitatively speaking, Eqs. (21)–(28) match both the data and the original Goda et al. (1975) design curves—which were obtained by digitizing the diagrams as presented in Goda (2000) (Figs. 7 and 8). Additionally, although Eqs. (21)–(28) were developed for conditions where $h_{toe}/H_{m0,deep} \leq 1$, the overtopping discharge for cases with $1 < h_{toe}/H_{m0,deep} \leq 1.5$ may also be well-estimated by taking the predicted maximum of Eqs. (21)–(28) (i.e., for $h_{toe}/H_{m0,deep} = 1$) (Figs. 7 and 8). It should also be noted that most of the data used to derive the EurOtop (2018) formulas for vertical structures start in this shallow range and extend to deeper conditions ($h_{toe}/H_{m0,deep} > 1$). This further highlights the significance of the Goda et al. (1975) data set and the need for formulas—such as Eqs. (21)–(28)—for shallower conditions.

Quantitatively, Eqs. (21)–(28) are unbiased with minor scatter, yielding an $\bar{x}_G$ value of 1.02 and $\sigma(\bar{x}_G)$ of 1.68. If we consider wave overtopping to be normally distributed, then 90% of the predicted overtopping discharge would be located within a range of values between 0.43 and 2.40 times the measured overtopping discharge. Furthermore, Fig. 9 shows that the ratio of the predicted [using Eqs. (21)–(28)] to measured overtopping discharge (q_{pred}/q_{meas}) is relatively uniform for varying values of $R_c/H_{m0,deep}$, $h_{toe}/H_{m0,deep}$, tan (m) and $s_{om-1,0}$. This condition, referred to as homoscedasticity, suggests that the accuracy of Eqs. (21)–(28) is not dependent on any single parameter. Fig. 9 also shows the parameter ranges used in the derivation of Eqs. (21)–(28), and hence, the ranges within which they can be reliably applied.

Sloping Structures

Using the same approach as outlined in the previous section "Vertical Structures" and the data sets listed in Table 2, the formulas derived for sloping structures with shallow foreshores follow:
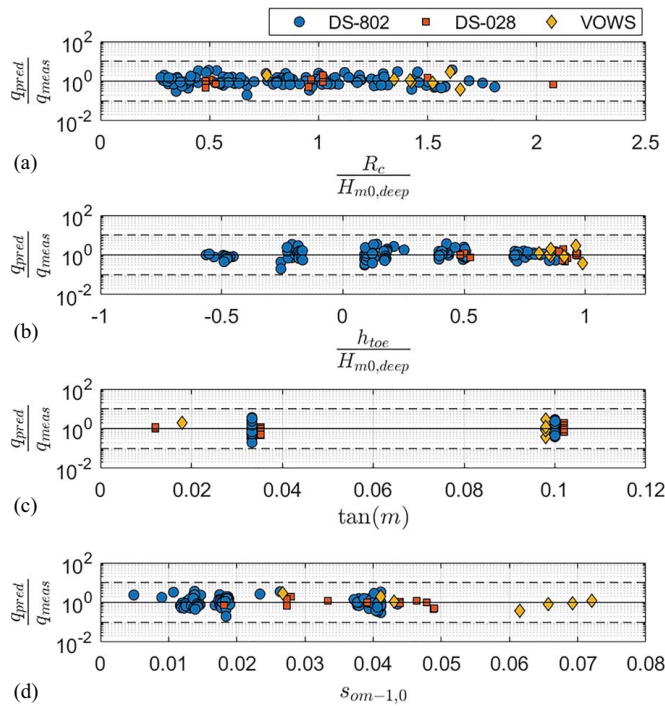
© ASCE

J. Waterway, Port, Coastal, Ocean Eng.

Fig. 9. Ratio of predicted [Eqs. (21)–(28)] to measured overtopping discharge (q_{pred}/q_{meas}) versus: (a) relative freeboard ($R_c/H_{m0,deep}$); (b) relative water depth ($h_{toe}/H_{m0,deep}$); (c) foreshore slope (tan (m)); and (d) wave steepness ($s_{om-1,0}$), for vertical structures (Table 3). The solid line indicates perfect agreement. Dashed lines represent predictions that are a factor of 10 higher/lower than measurements. Note that the data in panel c are slightly offset to make all points visible.

$$\frac{q}{\sqrt{g \cdot H_{m0,\text{deep}}^3}} = d \cdot \exp\left(-e \cdot \frac{R_c}{H_{m0,\text{deep}}} + f \cdot \frac{h_{\text{toe}}}{H_{m0,\text{deep}}}\right) \quad (29)$$

For very shallow cases (Regime 1), with $0.5 \leq h_{\text{toe}}/H_{m0,\text{deep}} \leq 1$:

$$d_1 = 1.90 \cdot s_{om-1,0}^{1.15} \quad (30)$$

$$e_1 = 7.40 \cdot \frac{s_{om-1,0}^{0.60}}{\tan (m)^{0.25} \cdot \tan (\alpha)^{0.60}} \quad (31)$$

and,

$$f_1 = 0.70 \cdot \frac{\tan (m)^{0.80}}{s_{om-1,0}^{0.80}} \quad (32)$$

For extremely shallow or emergent cases (Regime 2), with $h_{\text{toe}}/H_{m0,\text{deep}} \leq 0.1$:

$$d_2 = 1.35 \cdot \tan (m)^{0.35} \cdot s_{om-1,0}^{0.85} \quad (33)$$

$$e_2 = 3.75 \cdot \frac{s_{om-1,0}^{0.70}}{\tan (m)^{0.70} \cdot \tan (\alpha)^{0.60}} \quad (34)$$

and,

$$f_2 = 0.20 \cdot \frac{s_{om-1,0}^{0.35}}{\tan (m)^{1.30}} \quad (35)$$

with exponential interpolation between the two regimes ($0.1 < h_{\text{toe}}/H_{m0,\text{deep}} < 0.5$).
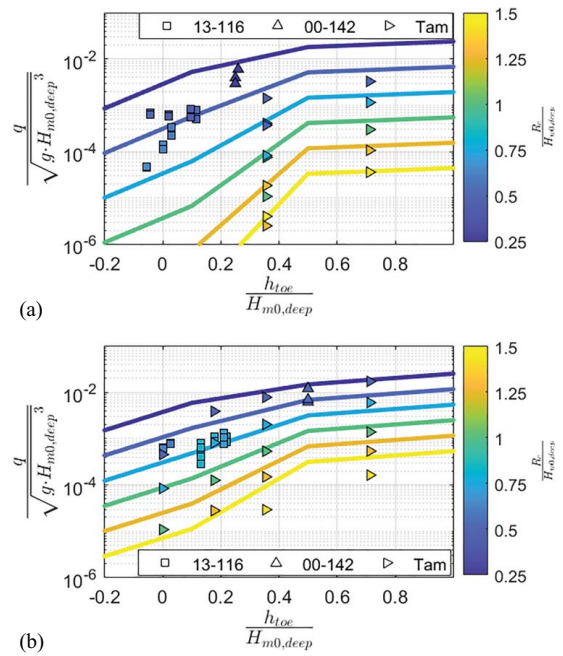

Fig. 10. Variation in relative discharge, $q/\sqrt{g \cdot H_{m0,\text{deep}}^3}$, with relative water depth ($h_{toe}/H_{m0,\text{deep}}$) and relative freeboard ($R_c/H_{m0,\text{deep}}$) for sloping structures (Table 2) with wave steepness ($s_{om-1,0}$): (a) 0.041; and (b) 0.018, for foreshore slopes (cot (m)) = 30 and 35 and structure slope (cot (α)) = 3. Solid lines represent Eqs. (29)–(35) with cot (m) = 32.5.

Eqs. (29)–(35) agree reasonably well with the data for sloping structures (Fig. 10) which show similar trends to those observed for vertical structures (Fig. 8). Figs. 11 and 12 also show no trend of increasing (or decreasing) scatter with changes in $R_c/H_{m0,\text{deep}}$, $h_{\text{toe}}/H_{m0,\text{deep}}$, tan ($m$), $s_{om-1,0}$, or tan (α), suggesting that homoscedasticity is maintained. It should be noted that due to the very small scale of the Tamada et al. (2002) data—with $0.027 \text{ m} \leq H_{m0,\text{deep}} \leq 0.068 \text{ m}$—there is larger inherent scatter in the observed overtopping discharge, compared with the other data sets (Figs. 11 and 12). Nevertheless, the Tamada et al. (2002) data set has been considered reliable because it was previously used to derive overtopping formulas (Goda 2009; Mase et al. 2013; Yuhi et al. 2020) and draw design diagrams [Figs. 5.8–5.10 in Goda (2010)].

Compared with the existing EurOtop (2018) approach [Eqs. (7)–(11)], Eqs. (29)–(35) show higher accuracy and a wider range of applicability. With $\bar{x}_G = 1.01$ and $\sigma(\bar{x}_G) = 1.90$, Eqs. (29)–(35) may be considered both accurate and unbiased, and if we consider wave overtopping to be normally distributed, then 90% of the predicted overtopping discharge would be located within a range of values between 0.35 and 2.92 times the measured overtopping discharge. On the contrary, the EurOtop (2018) formulas show a negative bias ($\bar{x}_G = 0.68$) and much larger scatter [$\sigma(\bar{x}_G) = 3.84$]—scatter which increases as the foreshore slope becomes steeper (Fig. 13). This is to be expected since the formulas were derived mainly for relatively mild foreshore slopes (Altomare et al. 2016). If we only consider the cases with cot (m) > 35, the accuracy of Eqs. (7)–(11) increases significantly ($\bar{x}_G = 1.11$ and $\sigma(\bar{x}_G) = 2.11$), thereby confirming their inapplicability to steeper foreshore slopes.

The new formulas proposed here [Eqs. (29)–(35)] may therefore be seen as an attractive alternative to Eqs. (7)–(11), when obtaining nearshore parameters is either impractical or would otherwise result
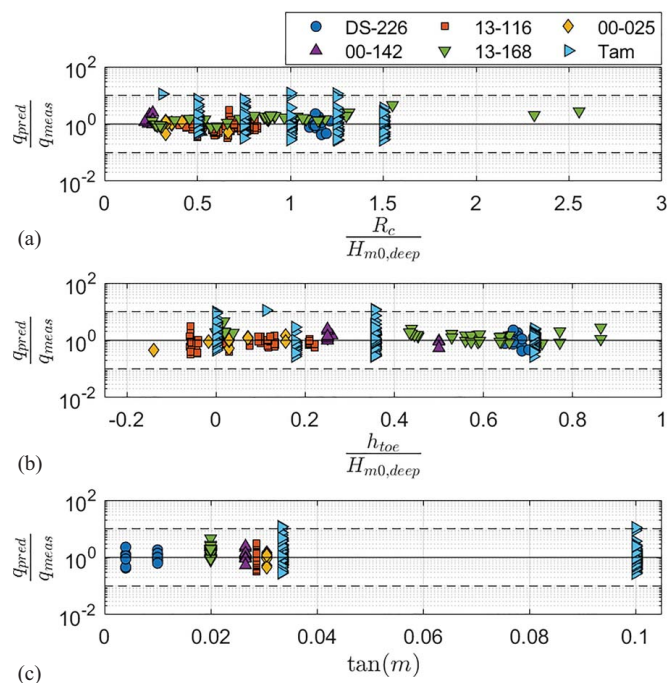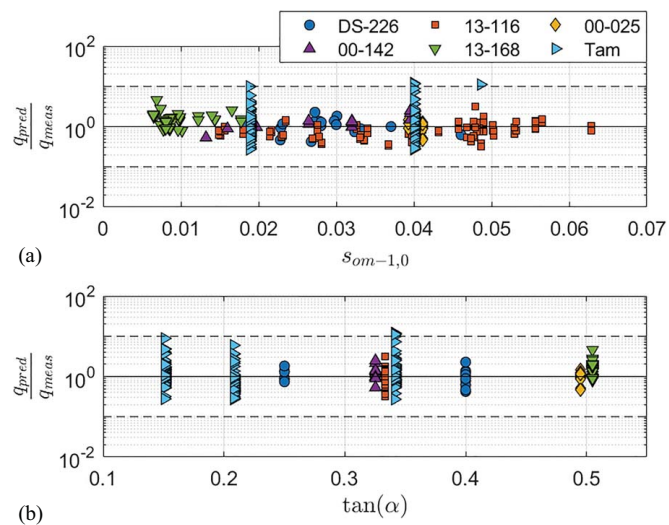
Fig. 11. Ratio of predicted [Eqs. (29) and (35)] to measured overtopping discharge (q_{pred}/q_{meas}) versus: (a) relative freeboard ($R_c/H_{m0,deep}$); (b) relative water depth ($h_{toe}/H_{m0,deep}$); and (c) foreshore slope (tan (m)) for sloping structures (Table 2). Solid line indicates perfect agreement. Dashed lines represent predictions that are a factor of 10 higher/lower than measurements. Note that the data for tan (m) = 0.029 (1:35 slope) are slightly offset to make all points visible.

Fig. 12. Ratio of predicted [Eqs. (29) and (35)] to measured overtopping discharge (q_{pred}/q_{meas}) versus: (a) wave steepness ($s_{om-1,0}$); and (b) structure slope (tan (α)), for sloping structures (Table 2). Solid line indicates perfect agreement. Dashed lines represent predictions that are a factor of 10 higher/lower than measurements. Note that the data for tan (α) = 0.33 and 0.5 are slightly offset to make all points visible.

in unwanted uncertainty. Furthermore, as the existing EurOtop (2018) formulas were mainly developed for relatively mild slopes (cot (m) $\geq$ 35); Eqs. (29)–(35)—which consider foreshore slopes as steep as 1:10—may prove further advantageous.
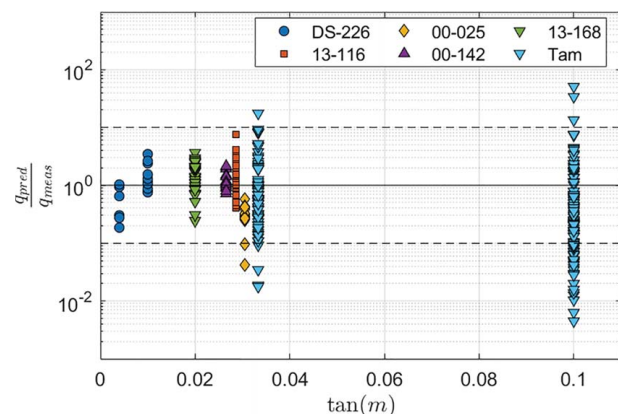

Fig. 13. Ratio of predicted [Eqs. (7)–(11)] to measured overtopping discharge versus foreshore slope (tan (m)) for sloping structures (Table 2). Solid line indicates perfect agreement. Dashed lines represent predictions that are a factor of 10 higher/lower than measurements. Note that the data for tan (m) = 0.029 (1:35 slope) are slightly offset to make all points visible.

Physical Explanation of the Proposed Empirical Coefficients

The coefficients of Eqs. (21)–(35) were established based on the observed influence of $s_{om-1,0}$, tan (α) and tan (m) on the mean overtopping discharge, while the values of their exponents were obtained using a trial-and-error approach to minimize scatter. Although the coefficients were the result of empirical fitting, their functional forms are in line with existing approaches which make use of a breaker parameter—which combines $s_{om-1,0}$, with either tan (α) (Van Gent 1999) or tan (m) (Bruce et al. 2004). The main difference here is the direct inclusion of both tan (m) and tan (α) compared with existing approaches that use a single imaginary or *equivalent* slope (Altomare et al. 2016; Mase et al. 2013).

Eqs. (21)–(35) show that $q/\sqrt{g \cdot H_{m0,deep}^3}$ increases as $s_{om-1,0}$ decreases (Fig. 14), consistent with the notion that longer waves yield larger overtopping volumes (EurOtop 2018). Likewise, the formulas also show that $q/\sqrt{g \cdot H_{m0,deep}^3}$ increases as the foreshore and structure slopes become steeper (Fig. 15), consistent with the early findings of Goda et al. (1975) and Owen (1980), respectively.

Considering the full range of structure slopes considered ($2 \leq$ cot (α) ≤ 7, Table 2), Figs. 14 and 15 show that $q/\sqrt{g \cdot H_{m0,deep}^3}$ is maximum at cot (α) = 2, but then reduces significantly for vertical structures (cot (α) = 0). Based on the work of Victor and Troch (2012) and Section 5.3.3 of EurOtop (2018) for less shallow water—who found that q indeed decreased from cot (α) = 2 to cot (α) = 0—interpolation between the formulas for vertical structures [Eqs. (21)–(28)] and those for sloping structures [Eqs. (29)–(35)] is recommended for very steep sloping structures (0 < cot (α) < 2). Curves for cot (α) = 1, obtained using this approach, are also shown in Figs. 14 and 15.

Limitations of the Approach

One notable limitation of the approach taken in the present study is the lack of data for validation. As data with shallow foreshores were limited, all of the available data were used to derive the expressions herein. Therefore, the accuracy of the formulas for conditions outside of the range used to derive them is unknown.

Second, while the approach based on deep-water wave characteristics has significant advantages, one drawback of this approach is the
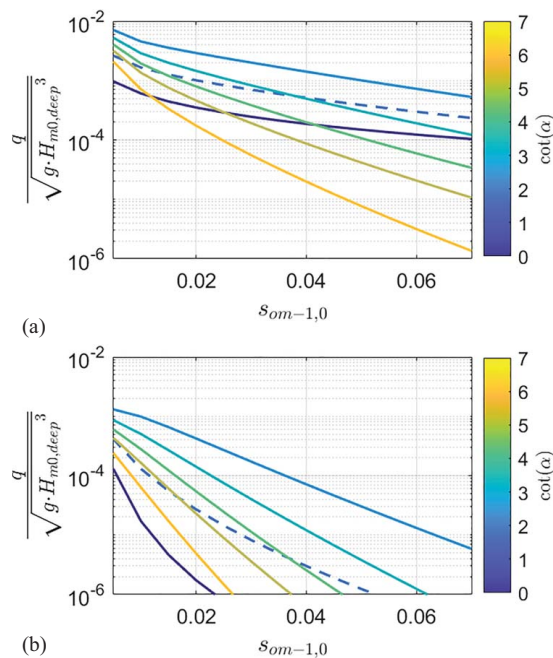
Fig. 14. Relationship between relative discharge, $q/\sqrt{g \cdot H_{m0,\text{deep}}^3}$, modeled using Eqs. (21)–(35) and wave steepness ($s_{om-1,0}$) for (a) very shallow conditions ($h_{\text{toe}}/H_{m0,\text{deep}} = 0.5$); and (b) extremely shallow conditions ($h_{\text{toe}}/H_{m0,\text{deep}} = 0.1$), for different structure slopes (cot (α)), with $R_c/H_{m0,\text{deep}} = 1$ and foreshore slope (tan (m) = 1:30). Dashed line for cot (α) = 1 was obtained by interpolating between formulas for vertical walls (cot (α) = 0) and sloping structures (cot (α) = 2).
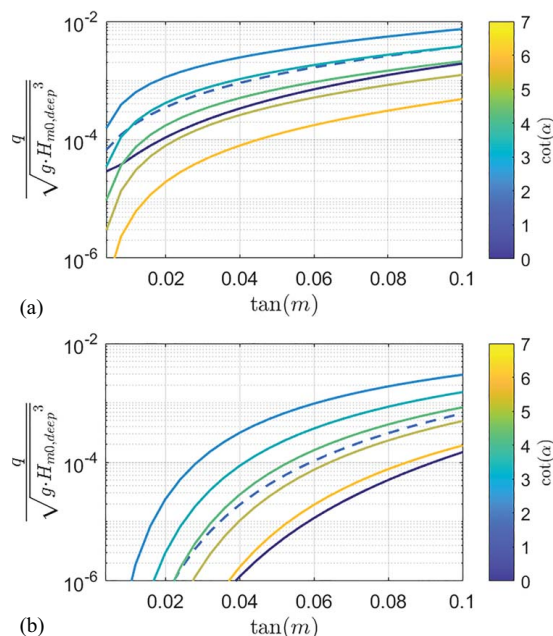
Fig. 15. Relationship between relative discharge, $q/\sqrt{g \cdot H_{m0,\text{deep}}^3}$, modeled using Eqs. (21)–(35) and foreshore slope (tan (m)) for (a) very shallow conditions ($h_{\text{toe}}/H_{m0,\text{deep}} = 0.5$); and (b) extremely shallow conditions ($h_{\text{toe}}/H_{m0,\text{deep}} = 0.1$), for different structure slopes (cot (α)), with $R_c/H_{m0,\text{deep}} = 1$ and wave steepness ($s_{om-1,0}$) = 0.03. Dashed line for cot (α) = 1 was obtained by interpolating between formulas for vertical walls (cot (α) = 0) and sloping structures (cot (α) = 2).

assumption of a uniform foreshore slope. In reality, foreshores may be very irregular with strong local variations in bed level, such as bars or ridges. Therefore, the formulas proposed here should be used with caution if applied to cases with highly irregular bathymetry.

Conclusions

A comprehensive collection of physical and numerical data sets was applied to (1) assess the influence of the foreshore on nearshore wave conditions; and (2) based on this assessment, derive empirical overtopping formulas for very shallow water up to emergent (initially dry) toes. In line with the work of Goda et al. (1975), we have shown that the effects of the foreshore can be well-represented by two foreshore parameters: $h_{\text{toe}}/H_{m0,\text{deep}}$ and tan (m). As such, it was possible to derive accurate overtopping formulas—for both vertical and sloping structures—which directly incorporate $h_{\text{toe}}/H_{m0,\text{deep}}$ and tan (m) to account for the changes that occur as a result of shallow foreshores. Findings suggest that relative magnitudes of wave-induced setup and IG waves at the toe of structures built on land or in extremely shallow water can be considerable, resulting in higher-than-expected overtopping.

The formulas developed for vertical structures [Eqs. (21)–(28)] provide an alternative to the original Goda et al. (1975) design diagrams for very shallow conditions ($h_{\text{toe}}/H_{m0,\text{toe}} \le 1$), where such a graphical approach may prove tedious or time-consuming. For sloping structures, the EurOtop (2018) approach is considered attractive from deep-to-shallow water ($h_{\text{toe}}/H_{m0,\text{toe}} > 1$)—where spectral wave models provide accurate estimates at the structure toe with little computational effort. However, Eqs. (29)–(35) provide an accurate and convenient alternate for very shallow conditions, where predicting wave parameters at the toe becomes highly uncertain or impractical (e.g., in the case of emergent toe conditions) without the use of computationally demanding, high-resolution numerical models.

While Eqs. (21)–(35) performed reasonably well here, their accuracy outside the range of conditions used to derive them has not been assessed (Figs. 9, 11, and 12 for an overview of parameter ranges). Furthermore, a drawback with formulas developed using deep-water wave parameters is the assumption of a uniform foreshore slope. Therefore, care should be taken when applying Eqs. (21)–(35) to cases with highly irregular bathymetry and numerical wave models [e.g., BOSZ (Lashley et al. 2020b)] should be used to verify results. Future work should extend the approach here by considering a wider range of foreshore slopes in the case of vertical structures and to even shallower (negative) water depths for sloping structures. Finally, more physical model tests focused on assessing wave setup and the magnitude of IG waves at the toe of structures built on land ($h_{\text{toe}}/H_{m0,\text{deep}} \le 0$) are needed to further support the findings presented here.

Data Availability Statement

All data, models, or code that support the findings of this study are available from the corresponding author upon reasonable request.

Acknowledgments

Notation

The following symbols are used in this paper:

$C_{\eta\eta}$ = wave-variance density (m²/Hz);

g = gravitational constant of acceleration (m²/s);

$H_{1/3}$ = significant wave height based on zero-crossing analysis (m);

H_{m0} = significant wave height, based on spectral moments $= 4\sqrt{\int_0^\infty C_{\eta\eta} df}$ (m);

$H_{m0,deep}$ = significant wave height offshore in deep water (m);

$H_{m0,toe}$ = significant wave height at the structure toe (m);

h_{toe} = initial water depth at the structure toe (m);

$L_{m-1,0}$ = wave length in deep water based on the spectral wave period (m);

m = foreshore slope angle (°);

q = mean wave overtopping discharge (m³/s/m);

R^2 = coefficient of determination (—);

R_c = crest freeboard (m);

$R_{u2\%}$ = 2% exceedance wave run-up (m) with respect to the number of incident waves;

$s_{om-1,0}$ = deep-water wave steepness based on the spectral wave period (—);

s_{op} = deep-water wave steepness based on the peak wave period (—);

$T_{1/3}$ = significant wave period (s) $\approx T_p/1.04$;

$T_{m-1,0,deep}$ = spectral wave period in deep-water (s) $\approx T_p/1.1$;

$T_{m-1,0,toe}$ = spectral wave period at the structure toe (s);

T_p = peak wave period in deep water (s);

$\bar{x}_G$ = geometric mean (—);

α = structure slope angle (°);

δ = equivalent slope, following Altomare et al. (2016) (—);

$\bar{\eta}$ = wave-induced setup (m);

$\xi_{m-1,0}$ = breaker index (Iribarren number) based on the spectral wave period and significant wave height at the structure toe (—); and

$\sigma(\bar{x}_G)$ = geometric standard deviation (—).

References

Altomare, C., X. Gironella, T. Suzuki, G. Viccione, and A. Saponieri. 2020a. "Overtopping metrics and coastal safety: A case of study from the Catalan coast." *J. Mar. Sci. Eng.* 8 (8): 556. https://doi.org/10.3390/jmse8080556.

Altomare, C., T. Suzuki, X. Chen, T. Verwaest, and A. Kortenhaus. 2016. "Wave overtopping of sea dikes with very shallow foreshores." *Coastal Eng.* 116: 236–257. https://doi.org/10.1016/j.coastaleng.2016.07.002.

Altomare, C., T. Suzuki, and T. Verwaest. 2020b. "Influence of directional spreading on wave overtopping of sea dikes with gentle and shallow foreshores." *Coastal Eng.* 157: 103654. https://doi.org/10.1016/j.coastaleng.2020.103654.

Battjes, J. A., and M. J. F. Stive. 1985. "Calibration and verification of a dissipation model for random breaking waves." *J. Geophys. Res.* 90 (C5): 9159–9167. https://doi.org/10.1029/JC090iC05p09159.

Bruce, T., J. Pearson, and W. Allsop. 2002. "Violent overtopping of seawalls-extended prediction methods." In *Breakwaters, Coastal Structures and Coastlines: Proc. Int. Conf. Organized by the Institution of Civil Engineers*, edited by N. W. H. Allsop, 245–255. London: Thomas Telford.

Bruce, T., J. Pearson, and W. Allsop. 2004. "Violent wave overtopping-extension of prediction method to broken waves." In *Coastal Structures 2003*, edited by J. A. Melby, 619–630. Reston, VA: ASCE.

Coates, T., R. Jones, and P. Bona. 1997. *Wind/swell seas and steep approach slopes*. Technical Rep. on Wave Flume Studies, TR24. Wallingford, UK: Hydraulic Research Institute Wallingford.

Dally, W. R. J. C. E. 1992. "Random breaking waves: Field verification of a wave-by-wave algorithm for engineering application." *Coastal Eng.* 16 (4): 369–397. https://doi.org/10.1016/0378-3839(92)90060-8.

EurOtop. 2018. "Manual on wave overtopping of sea defences and related structures. An overtopping manual largely based on European research, but for worldwide application." Accessed February 17, 2021. http://www.overtopping-manual.com.

Goda, Y. 1970. "Estimation of the rate of irregular wave overtopping of seawalls." [In Japanese.] *Rep. Port Harbour Res. Inst.* 9 (4): 3–41.

Goda, Y. 1985. *Random seas and design of maritime structures*. 1st ed. Tokyo: University of Tokyo Press.

Goda, Y. 2000. *Random seas and design of maritime structures. Vol. 15 of advanced series on ocean engineering*. 2nd ed. Singapore: World Scientific.

Goda, Y. 2009. "Derivation of unified wave overtopping formulas for seawalls with smooth, impermeable surfaces based on selected CLASH datasets." *Coastal Eng.* 56 (4): 385–399. https://doi.org/10.1016/j.coastaleng.2008.09.007.

Goda, Y. 2010. Vol. 33 of *Random seas and design of maritime structures*. 3rd ed. Singapore: World Scientific.

Goda, Y., Y. Kishara, and Y. Kamiyama. 1975. "Laboratory investigation on the overtopping rate of seawalls by irregular waves." [In Japanese.] *Rep. Port Harbour Res. Inst.* 14 (4): 3–44.

Herbert, D. 1993. *Wave overtopping of vertical walls*. Wallingford, UK: HR Wallingford.

Hofland, B., X. Chen, C. Altomare, and P. Oosterlo. 2017. "Prediction formula for the spectral wave period T m-1,0 on mildly sloping shallow foreshores." *Coastal Eng.* 123: 21–28. https://doi.org/10.1016/j.coastaleng.2017.02.005.

Lashley, C. H., J. D. Bricker, J. van der Meer, C. Altomare, and T. Suzuki. 2020a. "Relative magnitude of infragravity waves at coastal dikes with shallow foreshores: A prediction tool." *J. Waterw. Port Coastal Ocean Eng.* 146 (5): 04020034. https://doi.org/10.1061/(ASCE)WW.1943-5460.0000576.

Lashley, C. H., B. Zanuttigh, J. D. Bricker, J. van der Meer, C. Altomare, T. Suzuki, V. Roeber, and P. Oosterlo. 2020b. "Benchmarking of numerical models for wave overtopping at dikes with shallow mildly sloping foreshores: Accuracy versus speed." *Environ. Modell. Software* 130: 104740. https://doi.org/10.1016/j.envsoft.2020.104740.

Mase, H., and J. T. Kirby. 1993. "Hybrid frequency-domain KdV equation for random wave transformation." In *Coastal Engineering 1992*, edited by B. L. Edge, 474–487. Reston, VA: ASCE.

Mase, H., T. Tamada, T. Yasuda, T. S. Hedges, and M. T. Reis. 2013. "Wave runup and overtopping at seawalls built on land and in very shallow water." *J. Waterw. Port Coastal Ocean Eng.* 139 (5): 346–357. https://doi.org/10.1061/(ASCE)WW.1943-5460.0000199.

Owen, M. 1980. *Design of seawalls allowing for wave overtopping*. Rep. No. Ex 924. Wallingford, UK: HR Wallingford.

Pullen, T., and N. Allsop. 2004. *Final report on laboratory measurements Samphire Hoe*. CLASH WP4 D36. Wallingford, UK: HR Wallingford.

Sandoval, C., and T. Bruce. 2018. "Wave overtopping hazard to pedestrians: Video evidence from real accidents." In *Coasts, marine structures and breakwaters 2017: Realising the potential*, edited by K. Burgess, 501–512. London: ICE Publishing.

Smith, G., I. Wallast, and M. R. van Gent. 2003. "Rock slope stability with shallow foreshores." In *Coastal engineering 2002: Solving coastal conundrums*, edited by J. M. K. Smith, 1524–1536. Singapore: World Scientific.

Suzuki, T., C. Altomare, T. Yasuda, and T. Verwaest. 2020. "Characterization of overtopping waves on sea dikes with gentle and shallow foreshores." *J. Mar. Sci. Eng.* 8 (10): 752. https://doi.org/10.3390/jmse8100752.

Takayama, T., T. Nagai, and K. Nishida. 1982. "Decrease of wave overtopping amount due to seawalls of low crest types." [In Japanese.] *Rep. Port Harbour Res. Inst.* 21 (2): 151–205.

Tamada, T., M. Inoue, and T. Tezuka. 2002. "Experimental studies on diagrams for the estimation of wave overtopping rate on gentle slope-type seawalls and these reduction effects on wave overtopping." [In Japanese.] *Proc. Coastal Eng. JSCE* 49: 641–645. https://doi.org/10.2208/proce1989.49.641.

Tamada, T., H. Mase, and T. Yasuda. 2015. "Integrated formula of wave overtopping and runup modeling for vertical seawalls based on CLASH datasets." [In Japanese.] *J. Jpn. Soc. Civ. Eng., Ser. B2* 71 (2): 847–852. https://doi.org/10.2208/kaigan.71.I_847.

Van der Meer, J., and J. de Waal. 1993. *Waterbeweging op taluds: Invloed van berm, ruwheid, ondiep voorland en scheve lang-en kortkammige golfaanval*. [In Dutch.] Delft, Netherlands: Delft Hydraulics Laboratory.

Van Gent, M. 1999. *Physical model investigations on coastal structures with shallow foreshores: 2D model tests with single and double-peaked wave energy spectra*. Hydraulic Engineering Rep., Delft, Netherlands: Delft Hydraulics.

Victor, L., and P. Troch. 2012. "Wave overtopping at smooth impermeable steep slopes with low crest freeboards." *J. Waterw. Port Coastal Ocean Eng.* 138 (5): 372–385. https://doi.org/10.1061/(ASCE)WW.1943-5460.0000141.

Yuhi, M., H. Mase, S. Kim, S. Umeda, and C. Altomare. 2020. "Refinement of integrated formula of wave overtopping and runup modeling." *Ocean Eng.* 220: 108350. https://doi.org/10.1016/j.oceaneng.2020.108350.